Sensors and Actuators B 160 (2011) 318–326

Contents lists available at ScienceDirect

Sensors and Actuators B: Chemical

journal homepage: www.elsevier.com/locate/snb

Microfabricated electrochemical sensors for exhaustive coulometry applications

S. Carroll[a], M.M. Marei[a], T.J. Roussel[b], R.S. Keynton[b], R.P. Baldwin[a,*]

[a] Chemistry Department, University of Louisville, Louisville, KY, USA
[b] Bioengineering Department, University of Louisville, Louisville, KY, USA

ARTICLE INFO

Article history:
Received 17 May 2011
Received in revised form 14 July 2011
Accepted 26 July 2011
Available online 2 August 2011

Keywords:
Exhaustive coulometry
Thin-layer cell
Microfabrication
Electrode array

ABSTRACT

The development of microfabricated electrochemical systems suitable for deployment in sensor networks that operate with a minimum of operator intervention are of great interest; therefore, a coulometric sensing system for exhaustive coulometry with the potential for calibration-free operation has been designed, fabricated and evaluated to support such development. The sensor chips were microfabricated onto a silicon substrate and contained a variety of specially designed thin-film gold working electrodes (ranging from one to five per chip) and a Ag/AgCl pseudo-reference electrode. A custom flow cell containing fluidic connections and counter electrode chamber was also constructed to integrate the sensor and to create an electrolysis chamber with a fixed volume. Different chip designs were evaluated as exhaustive coulometric sensors in terms of reproducibility and longevity using $Fe(CN)_6^{3-/4-}$ as model analytes. The relative standard deviation (RSD) for a chip tested over a period of 42 days was 5.5% whereas the sensor-to-sensor reproducibility was within 6.3%.

1. Introduction

There currently exists a wide variety of environmental, industrial, and security applications where long-term remote chemical analysis is either required or at least highly desirable [1,2]. As a result, the design of "smart" sensors, capable of performing stable and reliable measurements without operator intervention has become an area of increasing interest in instrument and sensor development. At the same time, important progress has occurred in the microfabrication of analytical instruments and the production of so called "lab on a chip" (LOC) or "micro total analysis" (μTAS) systems. The benefit of miniaturization is not only smaller individual instruments but also the potential for incorporating multiple instruments on a single platform. The potential mass production of such miniaturized integrated measurement systems also allows, in principle, deployment of a network of devices which can simultaneously monitor many locations at once, especially when smart sensors that require little operator intervention are utilized. Consequently, it has been one of our group's objectives to investigate specific ways to utilize smart sensor design principles in conjunction with microfabrication.

Of course, there is a wide range of specific instrument characteristics that serve to make a sensor "smart". One approach to smart sensor design has been the inclusion of a number of independent sensor elements which are able to measure different sample attributes, as in μTAS [3–5]. The inclusion of redundant sensor elements for self-verification and the availability of back-up sensors for enhanced longevity is another approach [6]. A more difficult issue for operator-free smart sensors has been the issue of calibration. With the exception of a few commercial devices where a single sensor selected from a batch is used to initially calibrate the sensitivity of the entire lot [7], there have been very few examples of sensors which do not require at least an initial calibration. To our knowledge, there have been no reports of sensors which are capable of extended field operation without calibration, which is a challenging requirement even under the best circumstances. The response of most instruments is sufficiently unstable as to require at least periodic calibration, even under well controlled laboratory conditions. A sensor deployed in a truly remote setting is expected to experience a variety of physical conditions (temperature, humidity, etc.). Additionally, sample pretreatment and conditioning procedures are limited with a remote sensor.

There are several general approaches to solving the calibration problem, many of which lead to an increase in device cost and complexity. Device complexity in general leads to an increase in the frequency of failure, which in-turn requires more frequent maintenance. Collectively, additional costs reduce the practicality

* Corresponding author.
E-mail address: rick.baldwin@louisville.edu (R.P. Baldwin).

0925-4005/$ – see front matter © 2011 Elsevier B.V. All rights reserved.
doi:10.1016/j.snb.2011.07.055

of a large number of sensors in a network. We believe, a preferable approach is to identify and employ analytical measurement methods that are both compatible with field deployment and also provides absolute quantitative results and therefore can be considered "calibration free".

One analytical approach that is adaptable to large networks of remote sensors is electroanalysis. The theory of amperometry has been described for both flow-by and flow through sensors [8,9]. And amperometric sensors utilizing either flow-by or stopped flow analysis have been adapted to diverse applications including biosensing [10,11], gas sensing [12], chlorine [13]. However, all of the amperometric methods require calibration since the collected current depends on mass transport of the analyte (i.e. temperature, solvent viscosity, etc.) [14]. Amperometric measurements are also dependent on electrode area which may change with extended use due to fouling in a remote sensing application.

Of the electrochemical approaches for smart sensors, one that seems to have much to offer is coulometry [15] which is one of the few analytical methods that are capable of absolute quantitation. In principle, as long as the cell volume is accurately known and the electrolysis is carried out to completion, the corresponding charge is an absolute determinant of the analyte quantity and concentration. In addition, any changes in electrode area that occur over extended periods of operation, should be also less problematic; as long as the cell volume remains constant, partial passivation of the electrode surface affects the time dependence but not the magnitude of the coulometric signal.

In this work, we report on the development and evaluation of a first-generation microfabricated coulometric sensor system that we believe shows promise for calibration-free remote monitoring applications. Although there have been many examples of quantitative coulometry, few seem to be ideally suited remote monitoring applications. High surface area flow-through electrodes not only would require precise control of sample flow rate for reliable quantitation but also seem poorly suited to reproducible mass production. Rather, we have chosen to investigate the use of a small volume, thin-layer electrolysis cell employing readily fabricated planar electrodes. There are numerous examples that suggest that this approach has much to offer. For instance, Karube's group showed that a 45 μL thin-layer coulometric system constructed with a planar Cu anode permitted the measurement of chemical oxygen demand in lake water samples in a 3–10 min time frame [16]. Fukuda et al. described a micro-bulk electrolysis cell suitable for the study of mediated enzyme reactions and the relatively rapid coulometric analysis of the substrate species in 10 μL sample volumes [17]. Neither of these approaches was intended for, or applied to, remote sensing as both required extensive operator interaction. More recently, Bakker has shown that passage of controlled currents through ion selective membranes can be used to release precisely defined quantities of calcium and barium ions into the surrounding solution with high selectivity [18,19]. This approach offers the potential of carrying out a wide variety of calibration-free coulometric measurements that should eventually have interesting and useful applications in long-term remote sensing. In the current study, we report on the design, construction, and performance of a miniaturized sensor system intended to carry out exhaustive coulometric measurements and have eventual application in remote monitoring. The electrolysis chamber is a thin-layer cell, approximately 2.2 μL in volume, that contains working and reference electrodes microfabricated onto a silicon wafer and whose dimensions are defined by a silicone rubber gasket placed on top of the wafer. The working and counter electrode compartments are isolated by means of a semi-porous membrane that permits current flow but limits physical exchange between the two halves of the cell. Here we evaluate the performance of the coulometric sensor platform using ferri-/ferrocyanide as a model electrochemical analyte and describe the design considerations most critical for successful calibration-free operation.

2. Materials and methods

2.1. Reagents

For all coulometry experiments, potassium ferricyanide, potassium nitrate, and sodium chloride were purchased from Sigma–Aldrich (Milwaukee, WI) and potassium ferrocyanide from VWR International (Batavia, IL) at highest purity and were used without further purification. Analyte and electrolyte solutions were always freshly prepared using deionized (DI) water. A commercial silver plating solution (Technic Silver Cyless II RTU) obtained from Technic Inc., Cranston, RI was used to electroplate all reference electrodes.

2.2. Fabrication

2.2.1. Sensor

All sensor chips were fabricated in the cleanroom facility in the University of Louisville Center for Micro/NanoTechnology. The following discussion is intended to provide an overview of the fabrication process employed here. More detailed procedures are available upon request.

A 4-in. silicon wafer was employed as the substrate onto which different sensor designs were patterned via photolithography. The individual chip platforms were 1.3 cm wide × 2.1 cm long, with patterned gold electrodes occupying a 4 mm × 8 mm elliptical area near the center. Thus, 18 different chips could fit onto a single wafer and be fabricated together during each processing run.

Each chip contained from two to six independent gold electrodes, one of which was subsequently transformed into a Ag/AgCl pseudo-reference electrode. Fig. 1 shows the two different electrode schemes that were used in this work. The first (Design A) contained only two electrodes, a large Au oval with an area of 25.6 mm^2 surrounding a smaller Au strip with an area of 0.71 mm^2. The second (Design B) contained six 50 μm wide gold finger electrodes arranged in a concentric spiral pattern with an interelectrode spacing of 50 μm. The electro-active area of the working electrodes in Design B (W1–W5) was only 40.5% of the active working electrode area in Design A (W1). Details of the working electrode areas for electrodes on both chip designs are listed in Table 1.

The first step of the fabrication process consisted of growing a 600-nm thick oxide insulation layer onto the silicon wafer. Next, the desired pattern for the electrodes was transferred onto the wafer via photolithography and was etched into the wafer to a depth of ca. 250 nm using a buffered oxide etch. Subsequently, the electrodes were formed by sputtering a similar thickness of gold (preceded by a thin tantalum adhesion layer) so as to fill up the etched recesses. A lift-off procedure was used to remove the unwanted Au and leave the final electrode structures intact. A Disco DAD 321 dicing machine was then used to cleave the wafer into individual sensor chips.

Thereafter, one of the patterned Au electrodes on each chip was converted via electroplating to a Ag/AgCl pseudo-reference electrode. The procedure used to do this was similar to that reported by Shanthi [20]. First, the chip (R1, cathode) was placed into a commercial silver plating solution along with a Ag sputtered Si wafer (anode) where a 560-mV pulse train (40 ms on, 60 ms off) was applied for 70 min to give an initial current density of approximately 0.7 mA/cm^2. This current density slightly increased over time and was adjusted when necessary; exceeding 1.2 mA/cm^2 would lead to destruction of the gold electrode. Chlorination was then performed by placing the chip in a 1 M NaCl solution and

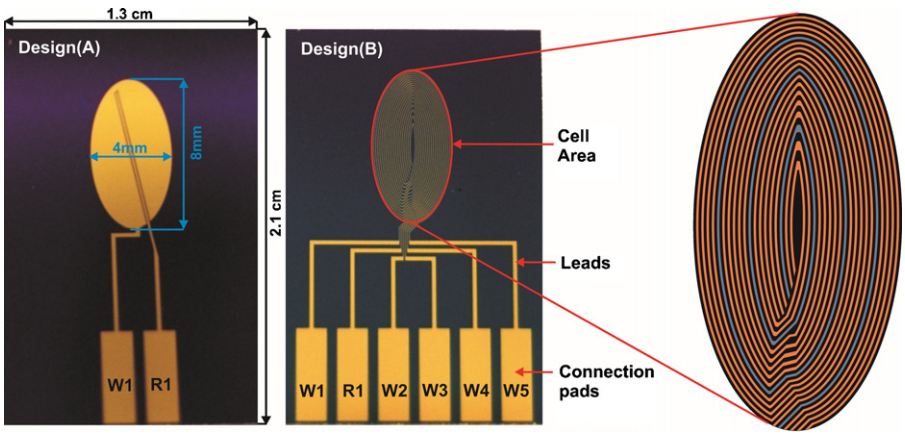

Fig. 1. Photographs illustrating two sensor chip layouts. Design (A) contains working electrode (W1) and reference electrode (R1), whereas Design (B) has five working electrodes (W1–W5) and one reference electrode (R1). Exploded view indicates detail of concentric spiral electrode design.

Table 1
Electrode areas of two sensor chips (Design A and B).

Design	W1 Area (mm^2)	W2 Area (mm^2)	W3 Area (mm^2)	W4 Area (mm^2)	W5 Area (mm^2)	R1 Area (mm^2)
(A)	25.6	–	–	–	–	.714
(B)	1.73	1.84	1.95	2.05	2.15	2.49

applying a 50-mV pulse train (40 ms on, 60 ms off) to the electroplated silver electrode (R1, anode) using a Pt wire (cathode) for 15 s.

2.2.2. Flow cell

The flow cell into which the microfabricated chips were inserted for analysis is shown in Fig. 2. It consisted of two principal pieces that were fabricated from Lexan by precision CNC milling. The microfabricated chips were placed onto the bottom Lexan piece into a shallow trench that had the same dimensions as the chip and acted as an alignment guide. The working electrode compartment of the electrochemical cell was formed by cutting an elliptical hole of the desired size into a 120 μm thick silicone rubber gasket and placing this gasket piece on top of the chip in the alignment trench. To isolate the working and counter electrode chambers, a semi-porous (200 Da) membrane (SelRO MPF-34, Koch Membrane System, Inc., Wilmington, MA) was placed over this bottom gasket layer. The volume and shape of the upper counter electrode chamber was defined by yet another silicone rubber gasket layer. To complete the three-electrode cell, a large surface-area gold wire counter electrode was inserted into the upper compartment through the top Lexan piece. The top and bottom sections were attached together by screws which facilitated reproducible alignment and could be tightened sufficiently to prevent leakage of solution from the cell compartment. Since knowledge of the precise volume of the working electrode chamber was required to carry out the intended coulometry experiments, membranes and gaskets were precision laser cut. In most of the coulometry experiments described below, the gaskets were cut so that the resulting sample volume of the working electrode chamber was calculated to be 2.2 μL (maximum range 2.17–2.29 μL). Averaged geometrical dimensions obtained by profilometric measurements on the cell assembly were used to calculate the cell volume.

2.3. Instrumentation

Pulsed potential silver depositions were carried out with a 5 MHz function generator (BK Precision 4011A), a multimeter (Agilent 34410A) and a digital oscilloscope (Rigol DS1052E). Electrochemical experiments were carried out using either a BASi epsilon potentiostat (Bioanalytical Systems, West Lafayette, IN) or a custom potentiostat designed in-house. The latter system, which utilized a LabVIEW (National Instruments, Austin, TX) interface designed to operate in one of many interrogation modes (coulometry, amperometry, potentiometry, cyclic voltammetry, etc.) for maximum flexibility in the field, was of interest because of our final goal of creating a field-deployable, automated detection system. All voltammetric and coulometric experiments used a three-electrode configuration with Au working, Ag/AgCl pseudo-reference, and Au wire counter electrodes. Analyte solutions for the electrolysis compartment and electrolyte solutions (0.1 M KNO_3) for the counter compartment solutions were introduced to the custom flow cell with a syringe.

3. Results and discussion

3.1. Design considerations

The specific cell design employed for this study was decided upon after considering various properties that were viewed as especially important in a prototype sensor that might be used for calibration-free analysis operations in the field. A critical characteristic for any viable coulometry measurement is, of course, that the cell volume is fixed. Further, it is necessary that this volume be readily determinable either by calculation from known cell dimensions or by initial calibration. A second critical issue is that the electrolysis process of interest needs to be carried out to completion within a reasonable/acceptable time frame. These two considerations led us to choose a thin-layer (<100 μm) cell design in which a large surface area working electrode would occupy the bottom surface of the coulometry compartment. Thus, the time required for complete electrolysis would depend solely on the analyte diffusion time across the narrow layer of solution above it. The time required for exhaustive electrolysis could be estimated from the average diffusion distance given by $(2Dt)^{1/2}$ where D represents the diffusion coefficient (cm^2/s) and t the time (s) [8].

Beyond this, the system should be comprised of a flow cell which enables convenient replacement of the sample solution without

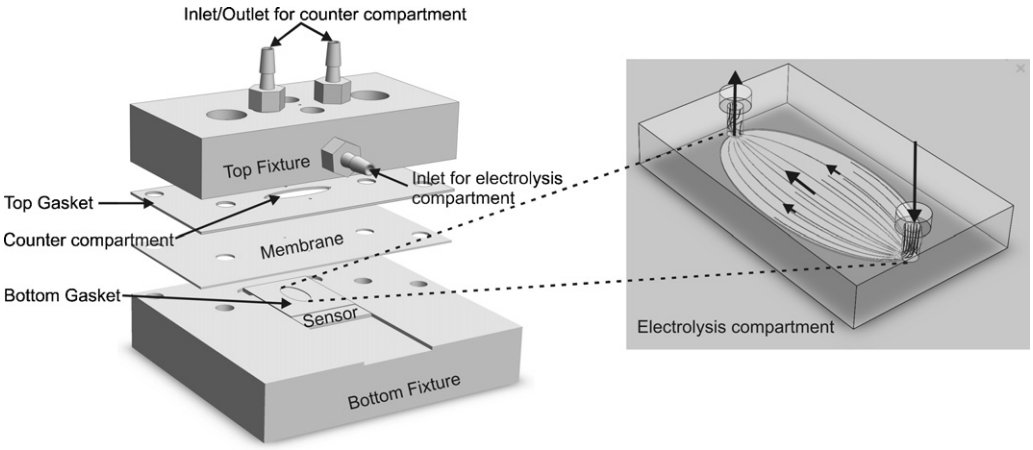

Fig. 2. Schematic view of the flow cell assembly. Inset shows isometric view of simulated laminar flow inside electrolysis compartment (8 mm × 4 mm × .08 mm).

manual dismantling of the cell. Additionally, the working electrodes ought to be isolated in a separate chamber in order to avoid possible interference from redox reactions occurring at the counter electrode. Finally, the microfabricated sensor chip itself should be able to be switched or replaced easily to allow different chips and electrode designs to be tested and compared.

After evaluating several different configurations in the early stages of this study, we settled on a single-gasket design with a 4 mm × 8 mm elliptical hole (i.e., cell) that covered the same area as the electrode pattern on the microfabricated chip. This elliptical shape was chosen in order to promote laminar flow of solution and complete clearing of the cell by eliminating corner areas where air bubbles and stagnant pools of sample might collect. The height of the alignment trench was chosen so that after assembly the cell thickness was 80 μm. With the compression needed to avoid leakage, the chip gasket creates a calculated nominal cell volume of 2.2 μL.

Microfabrication allows for the production of an essentially limitless number of electrode designs. In this work, the two specific electrode structures shown in Fig. 1 were employed. In the first, the chip contained only a single large working electrode (W1) that covered nearly the entire bottom side of the electrolysis compartment along with a pseudo-reference electrode (R1) embedded as a narrow strip spanning the middle of W1. In the second, the chip contained five independent working electrodes (W1–W5) arranged in a spiral pattern. This latter design was selected because it allowed us both to simulate a realistic sensing situation where the availability of several electrodes might be valuable and to select different electrode sizes and locations to obtain potentially useful information concerning the operation of the electrolysis cell. In all cases, for ease of fabrication, the material chosen for the surfaces of the microfabricated electrodes was Au. Although it will certainly be of interest in future studies to utilize additional working electrode materials, all the experiments described here used ferro-ferricyanide as a model analyte; and Au performed acceptably to carry out this redox process.

3.2. Chronoamperometry

Our basic experiment consisted of filling the working electrode compartment of the flow cell with an electroactive analyte species of known concentration and then stepping the applied potential to a value sufficient to cause the oxidation or reduction of this species; the electrode configuration used was normally that shown in Fig. 1 Design (A), with a single working electrode covering essentially the entire bottom surface of the cell. Fig. 3 shows the chronoamperograms obtained in this manner for a 250 μM ferrocyanide sample solution. The starting potential was −0.10 V, and the experiment was initiated by stepping to +0.40 V where the electro-oxidation to ferricyanide proceeded to completion. Subsequently, the applied

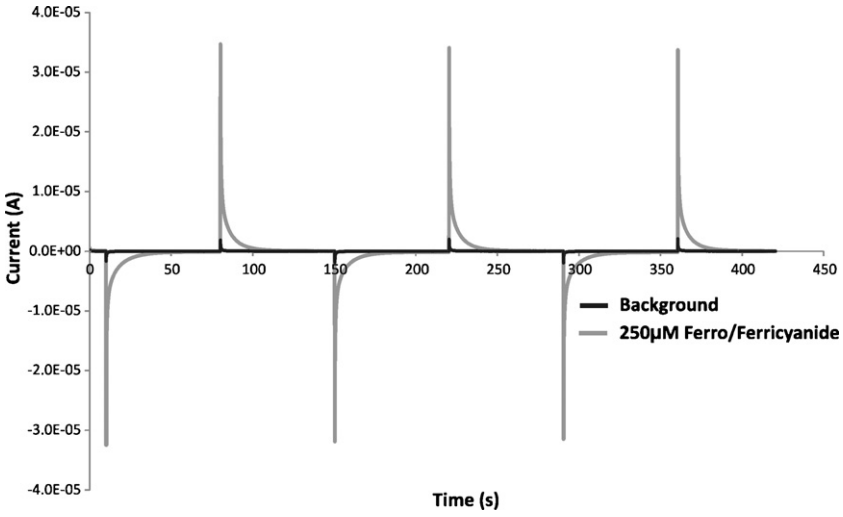

Fig. 3. Chronoamperograms of 250 μM $K_4Fe(CN)_6$ and the 0.1 M KNO_3 background for the thin-layer cell are obtained by pulsing between +0.4 V and −0.1 V vs. Ag/AgCl pseudo-reference.

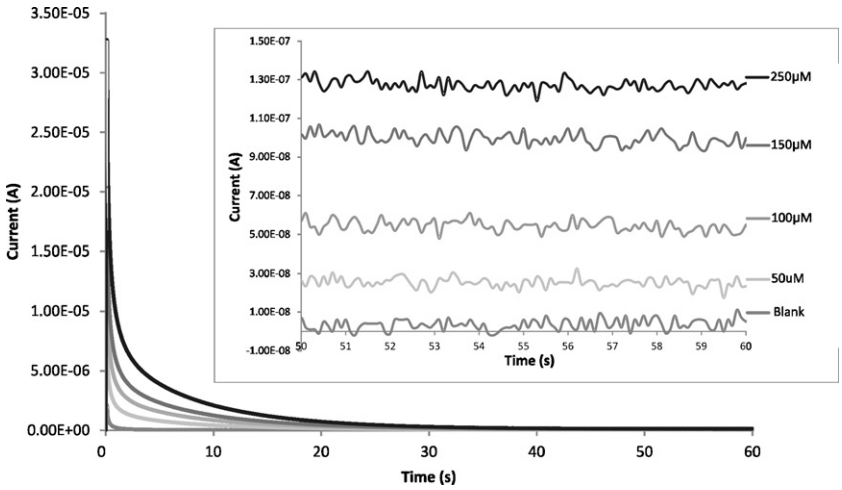

Fig. 4. Current time curves obtained for the thin-layer cell at 0.4 V vs. Ag/AgCl pseudo-reference for the background (0.1 M KNO_3), 50 μM, 100 μM, 150 μM and 250 μM $K_4Fe(CN)_6$ in 0.1 M KNO_3. A magnification of the ending current for the last 10 s is depicted in the inset.

potential was stepped back to −0.10 V in order to carry out the reverse redox process. (*Note*: these oxidation and reduction potentials were established earlier via cyclic voltammetry performed on an $Fe(CN)_6^{3-/4-}$ solution under the same solution/electrode conditions.) As can be seen from the figure, each change in potential produced an immediate spike in current, anodic for the positive potential and cathodic for the negative, which decayed to near background within less than 30 s. Each current spike was nearly equal in size, and the potential pulsing could be continued indefinitely with little or no change in the magnitude of the current spikes. When the identical experiment was carried out with a blank electrolyte solution, only a much smaller and more rapidly decaying current was observed, presumably due to charging current. Furthermore, when the same experiment was performed on solutions of different $Fe(CN)_6^{4-}$ concentrations, the amplitude of the current spikes was seen to track directly with this concentration, as shown in Fig. 4. All these chronoamperometric observations were consistent with the reversible oxidation and reduction of ferroferricyanide in a thin-layer cell. Furthermore, the time frame of the current spikes following each potential step matched reasonably well the roughly 5-s average diffusion time estimated for the 80-μm thickness of our specific cell.

A closer look at the corresponding amperograms (as shown in the Fig. 4 inset) revealed that, although nearly all of the electrolysis current had dissipated within 30 s after application of the electrolysis potential, there remained a very small but still significant current that was clearly above the background level and persisted throughout the entire measurement period. In fact, this long-term current decreased in magnitude only extremely slowly and persisted at an above-background level for several minutes. In addition, the magnitude of this long-lived current was directly related to the specific $Fe(CN)_6^{3-/4-}$ concentration employed.

One possibility for this observation was an appreciable diffusion of $Fe(CN)_6^{3-/4-}$ analyte from the channels used to allow flow of the sample solution into and out of the electrolysis chamber. In our device, these consisted of pinhole-sized (500-μm diameter) openings which had been laser-cut through the membrane and gasket layers used to isolate the top and bottom cell compartments. These channels remained open to the electrolysis cell and contained sample solution throughout the analysis. Complications arising from this condition have been reported in earlier thin-layer spectroelectrochemistry experiments [21] where it was shown that accurate coulometry depended on properly restricting inlet and outlet dimensions. In order to investigate this possibility, we compared the experimental *i*–*t* curve obtained for electrolysis of 100 μM $Fe(CN)_6^{4-}$ with a calculated model of unrestricted linear diffusion (i.e., the Cottrell equation) and a model for a thin-layer cell of 80 μm thickness. For these calculations, a diffusion coefficient of 0.667×10^{-5} cm^2/s was employed [22]. Direct comparison to the Cottrell and thin-layer models shows the experimental results are intermediate in nature (Fig. 5A). At short times, where the main contributor to the current is oxidation of the $Fe(CN)_6^{4-}$ present initially in the cell, the signal closely matches the initial rapid decay calculated for an ideal thin-layer cell. However, after 3–4 s, the presence of a more slowly decreasing component is evident. We suspect that this longer-lived current, which is present throughout the 60-s measurement period but is always well below the predicted semi-infinite diffusion conditions assumed in the Cottrell analysis, is due

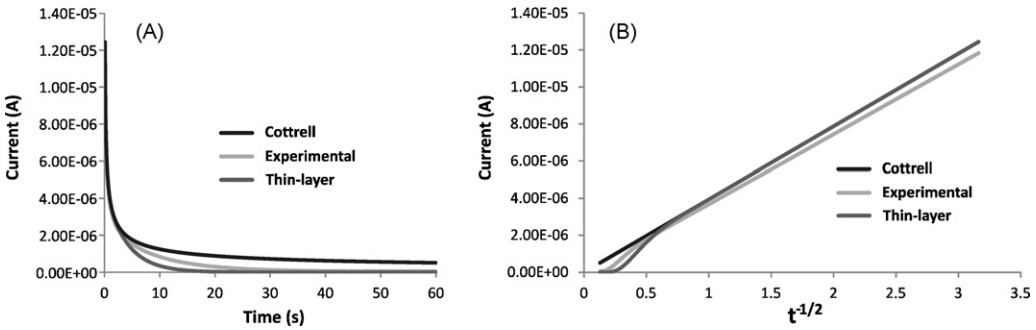

Fig. 5. Current time plots (A) for calculated unrestricted linear diffusion (Cottrell), experimental data (for the oxidation of 100 μM $K_4Fe(CN)_6$), and a thin-layer cell. The corresponding Cottrell plots are depicted in (B).

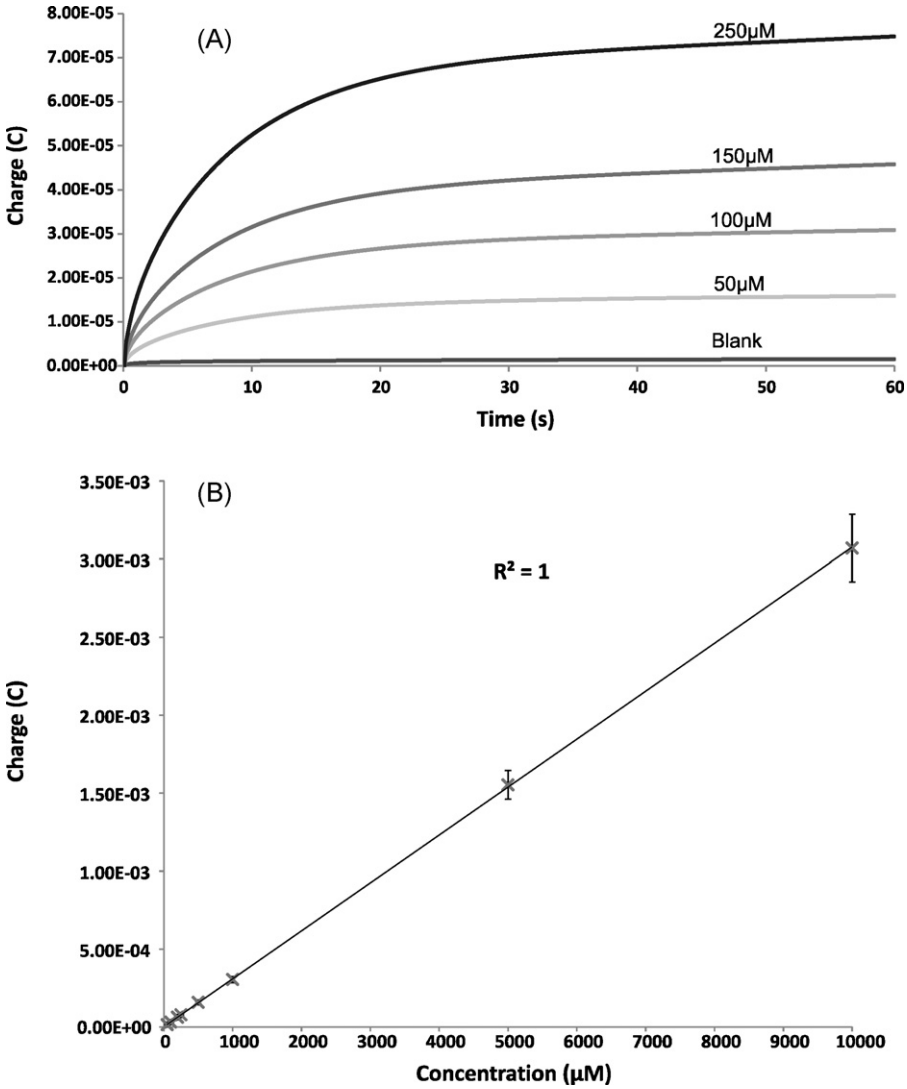

Fig. 6. Charge time curves (A) for the background (0.1 M KNO_3), 50 μM, 100 μM, 150 μM and 250 μM $K_4Fe(CN)_6$ in 0.1 M KNO_3. Calibration curve (B) is generated from 60 s electrolysis data which were obtained over three different days for 50/100/200/250/500/1000/5000 and 10,000 μM $K_4Fe(CN)_6$ in 0.1 M KNO_3 where $n = 9$ for each concentration.

at least in large part to diffusional leakage of $Fe(CN)_6^{4-}$ into the cell from its inlet and outlet channels. Classic Cottrell plots (i vs. $t^{-1/2}$) (Fig. 5B) showed two linear regions, one at times less than 5 s, corresponding to diffusion in the volume of the thin-layer cell, and the other at longer times due, presumably, to diffusion from the inlet and outlet channels. The initial magnitude and slope of the experimental data both deviate from the Cottrell/thin-layer theoretical values due to non-ideal limitations in data acquisition such as electronic transient response characteristics and noise filtering circuitry.

Regardless of the specific explanation for the extra current in the greater than 5 s regime, it seems clear that our electrolysis cell is not behaving exactly as an ideal thin-layer device, and we believe that a major contributor to this deviation is the relatively slow diffusion of analyte into the cell from the sample inlet and output channels. In the next flow cell design, it will be important to avoid, or at least minimize, this issue by decreasing the size of these channels. A distinct strength of the microfabrication approach to instrument construction is the number and variety of design changes that can be made with μm channel dimensions. Even complex designs can be executed with a high degree of fidelity.

3.3. Coulometry

The specific goal of this work was to evaluate exactly how well the microfabricated cell system behaved coulometrically. Therefore, the i–t data shown in Fig. 4 for different $Fe(CN)_6^{4-}$ concentrations were integrated to produce the corresponding q–t results shown in Fig. 6. Again, the results obtained were qualitatively as expected. The initial rapid increase in charge, corresponding to the electrolysis of the primary sample, was largely completed and the cumulative charge leveled off within 20–30 s. Further, the charge tracked the $Fe(CN)_6^{4-}$ concentration closely over a very wide range −50 μM to at least 10,000 μM in this set of experiments.

However, detailed inspection of the figure confirms that the charge did not actually reach a constant value even at long times but rather continued to increase slowly at steady rate. This can be most easily seen for the q–t curves generated for the higher $Fe(CN)_6^{4-}$ concentrations; but, as shown by the numerical data in Table 2, this phenomenon occurred at the same extent for all concentrations. Of course, in view of the fact that the electrolysis current did not decay to the background level within the time frame of the experiment, the accumulated charge must continue to increase slowly as

Table 2
Charge responses for the reduction/oxidation of ferri-/ferrocyanide at different concentrations and times. Data is reported along with the standard deviation (*n* represents the number of different days).

	Expected charge (μC)	Charge after 10 s	Charge after 30 s	Charge after 60 s
Reductions				
50 μM (*n* = 4)	10.61	9.71 (±0.47)	12.56 (±0.72)	13.50 (±1.19)
100 μM (*n* = 4)	21.23	20.33 (±0.54)	26.50 (±0.58)	28.28 (±0.66)
150 μM (*n* = 4)	31.84	30.78 (±0.99)	40.40 (±1.54)	42.88 (±1.23)
250 μM (*n* = 4)	53.07	51.30 (±2.41)	67.37 (±4.38)	71.30 (±4.58)
Oxidations				
50 μM (*n* = 5)	10.61	9.95 (±0.89)	13.45 (±1.16)	14.68 (±1.50)
100 μM (*n* = 5)	21.23	20.57 (±1.10)	27.92 (±1.61)	30.3 (±2.09)
150 μM (*n* = 3)	31.84	31.25 (±0.71)	42.31 (±1.92)	46.47 (±2.49)
200 μM (*n* = 2)	42.45	41.51 (±1.79)	56.46 (±1.68)	60.53 (±1.82)
250 μM (*n* = 5)	53.07	51.97 (±0.58)	69.88 (±1.29)	75.32 (±1.87)

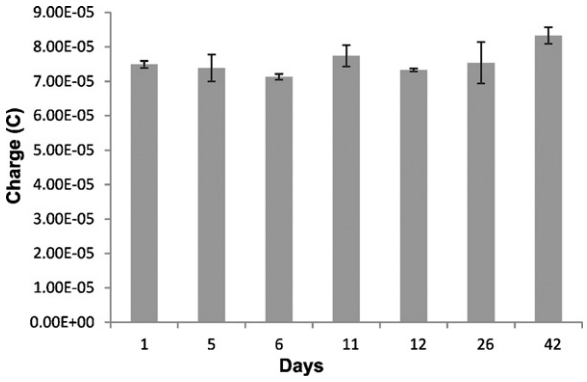

Fig. 7. Coulometric responses obtained from one chip over a period of 42 days at a 250 μM $K_4Fe(CN)_6$ in 0.1 M KNO_3. The total charge obtained after 60 s is background corrected and reported along with the standard deviation where *n* = 3.

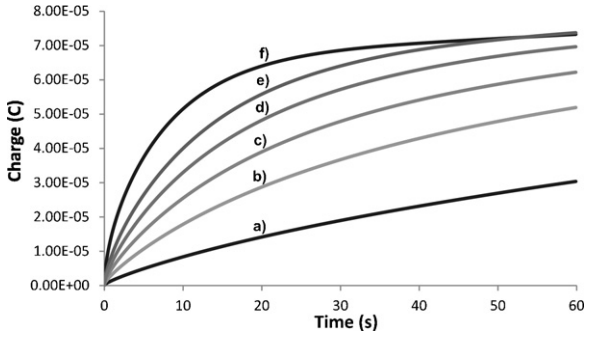

Fig. 8. Background corrected charge time curves for a Design (B) sensor where the charge for the oxidation of 250 μM $K_4Fe(CN)_6$ was obtained for one (a), two (b), three (c), four (d), and five (e) connected electrodes. Trace f represents the charge for a Design (A) chip at the same $K_4Fe(CN)_6$ concentration.

well. The table also shows the total charge calculated from Faraday's law for each concentration for the 2.2 μL volume of the cell compartment. In every case, these target values were consistently reached within 10–15 s of the start of the electrolysis. This time frame was the same for every concentration used and also for both the $Fe(CN)_6^{3-/4-}$ oxidation and reduction processes.

One of the most attractive features of the coulometric measurement approach for applications involving remote or unattended monitoring experiments should be its reliability over time and its freedom from many specific operational variables. With this in mind, we examined the performance of our device over a 6–7 week period. Results obtained with the same microfabricated chip for 250-μM $Fe(CN)_6^{4-}$ over this period are shown in Fig. 7. The data shown for seven typical sets of runs spanning this length of time gave a relative standard deviation (RSD) of only 5.5%. During the course of the testing period, nearly 500 individual electrolysis experiments were conducted on this chip; and the entire cell was assembled and disassembled numerous times. In addition, no special cleaning or treatment procedures beyond occasional rinsing with water and ethanol were applied to the electrodes. There was no deterioration of the device, and presumably the evaluation could have been extended to a longer testing period if we had so desired. The variability between different microfabricated chips (RSD = 6.3%; *n* = 3) was essentially the same as seen above for different sets of experiments carried out on the same chip.

All of the amperometry and coulometry results described so far involved the use of the microfabricated chip with the simple electrode configuration shown in Fig. 1 Design (A). Beyond this, we chose to carry out some additional experiments with a chip with the more complicated electrode pattern shown in Fig. 1 Design (B). Initially, this arrangement, containing six independent spiral-shaped finger electrodes, was designed to demonstrate the capability of incorporating several redundant working electrodes in the same device. However, it also proved informative with respect to the device's coulometric operation as well. In particular, the electrode area could be minimized (and the analyte diffusion distances maximized) by using only a single finger electrode to carry out the electrolysis. Alternatively, an increasing number of electrodes could be connected together so as to systematically increase the working electrode area thereby shorten the diffusion distance between individual electrodes and gradually approximate the single large electrode model.

Shown in Fig. 8 (traces a–e) are the results of coulometry experiments when one–five finger electrodes were employed to carry out the $Fe(CN)_6^{4-}$ reduction. Shown for comparison in trace f is a *q*–*t* curve that was obtained when a single large working electrode (as in Fig. 1A) was used. Clearly, when a single finger electrode (trace a) was employed the charge accumulated much more slowly and was less than half the total seen for the large electrode after a 1-min electrolysis. In fact, even when the electrolysis was allowed to proceed for 5 min, the charge with the single finger electrode remained well below that seen for the large electrode. As the number of finger electrodes linked together was increased, the rate of charge build-up increased as well. But only when all five fingers were employed simultaneously (see trace e) was the charge able to catch up with that seen for the large electrode within the 60-s time frame. Even in this instance, the $Fe(CN)_6^{4-}$ electrolysis occurred at a somewhat slower rate initially due to the smaller electrode coverage and the resulting larger diffusion distance still in effect. When evaluating the specific layouts for the five different electrode arrangements, it becomes clear that the maximum diffusion distance is no longer the cell height of 80 μm. Using the average diffusion distance calculation, the time required to complete electrolysis should increase by a factor of 1.25, 6.25, 14, 25, and 56 for the five, four, three, two and one electrode arrangements, respectively, when compared to the large electrode. By decreasing the number of electrodes, measurement of the Faradaic current

may be enhanced through a reduction of the background current, with an associated lowered detection limit. However, the practicality of this approach should be contrasted with the increased time necessary to complete the electrolysis for increased diffusion distances.

These results show that, although it is certainly possible to include in one chip multiple independent electrodes that might be useful in various applications, the particular electrode arrangement in Fig. 1B seems not to be the ideal one for carrying out rapid coulometric measurements. However, it is apparent that creation and operation of a complex microfabricated electrode scheme is readily achievable. Beyond this, the results in Fig. 8 serve to demonstrate another likely advantage of the coulometric approach for remote monitoring applications – namely, a substantial freedom from partial fouling or de-activation of the electrode surface. In conventional amperometric or voltammetric approaches, the critical quantity measured is the current whose magnitude is directly tied to electrode area. Thus, dependable performance with real samples over an extended period of time often requires periodic restoration of the working electrode surface. In the laboratory, this can be accomplished by manual, chemical, and electrochemical procedures, all of which would be troublesome, if not impossible, without extensive operator interactions. Coulometry, on the other hand, still offers the possibility of accurate and reproducible results for a partially passivated electrode surface by simply allowing more time for the electrolysis process to reach completion. For example, for curve e in Fig. 8 where the area of all the connected finger electrodes is only 40.5% of that of the large single electrode used for curve f, the measured charge has already caught up within less than 1 min.

4. Conclusions

This study has demonstrated many of the potential advantages of developing microfabricated coulometric devices for remote monitoring applications. By use of low-volume thin-layer cells, exhaustive electrolysis can be carried out on the time scale of a minute or less and can be repeated for weeks with highly reproducible results. Most important, reliable quantitative results can be obtained over a very wide concentration range in a calibration-free manner that offers the possibility of long-term unattended operation. A second-generation device that allows the cell volume to be defined absolutely and, in particular, minimizes analyte entry by diffusion from the inlet and outlet channels is presently under development in our laboratory, and we hope to report on this device and its performance in realistic applications shortly.

Acknowledgements

The authors would like to acknowledge Dr. Cindy Harnett and Evgenia Moiseeva (University of Louisville) for their assistance with the laser cutting process and Douglas Jackson (University of Louisville) for analog circuit design and discussions. This work was supported by the University of Louisville Research Incentive Funds Program, and the Lutz Endowment in the Department of Bioengineering at the University of Louisville.

References

[1] D. Diamond, S. Coyle, S. Scarmagnani, J. Hayes, Wireless sensor networks and chemo-/biosensing, Chem. Rev. 108 (2008) 652–679.
[2] P. Namour, M. Lepot, N. Jaffrezic-Renault, Recent trends in monitoring of European water framework directive priority substances using micro-sensors: a 2007–2009 review, Sensors-Basel 10 (2010) 7947–7978.
[3] D. Quinton, A. Girard, L.T.T. Kim, V. Raimbault, L. Griscom, F. Razan, S. Griveau, F. Bedioui, On-chip multi-electrochemical sensor array platform for simultaneous screening of nitric oxide and peroxynitrite, Lab Chip 11 (2011) 1342–1350.
[4] C. Ritter, F. Heike, K. Herbert, K.F. Josef, L. Susanne, N. Christian, O. Helmut, P. Gabriele, S. Bernhard, S. Marieluise, S. Wolfgang, S. Gregor, Multiparameter miniaturised sensor arrays for multiple use, Sens. Actuators B: Chem. 76 (2001) 220–225.
[5] W. Vonau, F. Gerlach, S. Herrmann, Conception of a new technique in cell cultivation using a lab-on-chip aided miniaturised device with calibratable electrochemical sensors, Microchim. Acta 171 (2010) 451–456.
[6] S. Carroll, R.P. Baldwin, Self-calibrating microfabricated iridium oxide pH electrode array for remote monitoring, Anal. Chem. 82 (2010) 878–885.
[7] A. Heller, B. Feldman, Electrochemical glucose sensors and their applications in diabetes management, Chem. Rev. 108 (2008) 2482–2505.
[8] A.J. Bard, L.R. Faulkner, Electrochemical Methods: Fundamentals and Applications, 2nd ed., John Wiley, New York, 2001.
[9] D.I. Vaireanu, N. Ruck, P.R. Fielden, Predictive model for coulometric operation in a thin-layer amperometric flow cell, Anal. Chim. Acta 306 (1995) 115–122.
[10] S.V. Dzyadevych, V.N. Arkhypova, A.P. Soldatkin, A.V. El'skaya, C. Martelet, N. Jaffrezic-Renault, Amperometric enzyme biosensors: past, present and future, Irbm 29 (2008) 171–180.
[11] N.J. Ronkainen, H.B. Halsall, W.R. Heineman, Electrochemical biosensors, Chem. Soc. Rev. 39 (2010) 1747–1763.
[12] X.J. Huang, L. Aldous, A.M. O'Mahony, F.J. del Campo, R.G. Compton, Toward membrane-free amperometric gas sensors: a microelectrode array approach, Anal. Chem. 82 (2010) 5238–5245.
[13] F.J. Del Campo, O. Ordeig, F.J. Munoz, Improved free chlorine amperometric sensor chip for drinking water applications, Anal. Chim. Acta 554 (2005) 98–104.
[14] S. Tsujimura, A. Nishina, Y. Kamitaka, K. Kano, Coulometric D-fructose biosensor based on direct electron transfer using D-fructose dehydrogenase, Anal. Chem. 81 (2009) 9383–9387.
[15] E. Bakker, V. Bhakthavatsalam, K.L. Gemene, Beyond potentiometry: robust electrochemical ion sensor concepts in view of remote chemical sensing, Talanta 75 (2008) 629–635.
[16] K.H. Lee, T. Ishikawa, S. Sasaki, Y. Arikawa, I. Karube, Chemical oxygen demand (COD) sensor using a stopped-flow thin layer electrochemical cell, Electroanalysis 11 (1999) 1172–1179.
[17] J. Fukuda, S. Tsujimura, K. Kano, Coulometric bioelectrocatalytic reactions based on NAD-dependent dehydrogenases in tricarboxylic acid cycle, Electrochim. Acta 54 (2008) 328–333.
[18] V. Bhakthavatsalam, A. Shvarev, E. Bakker, Selective coulometric release of ions from ion selective polymeric membranes for calibration-free titrations, Analyst 131 (2006) 895–900.
[19] E. Grygolowicz-Pawlak, E. Bakker, Background current elimination in thin layer ion-selective membrane coulometry, Electrochem. Commun. 12 (2010) 1195–1198.
[20] C. Shanthi, S. Barathan, R. Jaiswal, R.M. Arunachalam, S. Mohan, The effect of pulse parameters in electro deposition of silver alloy, Mater. Lett. 62 (2008) 4519–4521.
[21] D.A. Condit, M.E. Herrera, M.T. Stankovich, D.J. Curran, 5-Electrode thin-layer cell for spectroelectrochemistry applied to spectrocoulometric titrations, Anal. Chem. 56 (1984) 2909–2914.
[22] S.J. Konopka, B. Mcduffie, Diffusion coefficients of ferricyanide and ferrocyanide ions in aqueous media, using twin-electrode thin-layer electrochemistry, Anal. Chem. 42 (1970) 1741–1746.

Biographies

Susan Carroll is currently a Ph.D. candidate in Chemistry at the University of Louisville. She received her B.S. in Chemical Science (2004) from the Kansas State University and her M.S. in Chemistry (2009) from the University of Louisville. Her electroanalytical chemistry research focus is on the development, fabrication and electrochemical detection/modification of microfabricated devices.

Mohamed Marei received his B.S. in Chemistry (2006) and M.S. in Biochemistry (2009) from the University of Cincinnati. He is currently pursuing a Ph.D. Degree at the University of Louisville with a research focus on microfabricated electrochemical sensors which are suitable for calibration-free and remote sensing.

Thomas J. Roussel, Jr. is currently a Ph.D. candidate in Mechanical Engineering at the University of Louisville. He received the B.A. degree in Chemistry from the University of New Orleans in 1993, and the B.S. and M.S. degrees in Biomedical Engineering from Louisiana Tech University in 1997 and 2001, respectively. Since 2001, he has been a full-time research scientist in the Bioengineering Department at the University of Louisville. His research includes physical computing, microfluidics and Lab-on-a-Chip devices, analytical chemistry detection methodologies, finite element/finite volume analysis, and instrumentation/control systems.

Robert S. Keynton is currently chair, professor and Lutz Endowed Chair of Biomechanical Devices of the Department of Bioengineering at the University of Louisville. He received the B.S. degree in engineering science and mechanics from Virginia Tech in 1987, the M.S. and Ph.D. degrees in biomedical engineering from the University of Akron in 1990 and 1995, respectively. From 1995 to 1998, he worked at Louisiana Tech University as an assistant professor. Since 1999, he has been a faculty member at the University of Louisville. His research focuses on BioMEMS, microfluidics, Lab-

on-a-Chip devices, nanofabrication, MEMS modeling, micromechanical machining, and cardiovascular mechanics.

Richard P. Baldwin received his B.A. in Chemistry from Thomas More College in 1970 and his Ph.D. in Analytical Chemistry from Purdue University in 1976. He then joined the faculty of the University of Louisville where he is currently Professor of Chemistry. Since 2000, he has served as an Editor of *Analytica Chimica Acta*. His research interests have included numerous aspects of electroanalytical chemistry – most recently, microfabricated electrochemical instrumentation, lab-on-a-chip devices, and analytical systems for remote monitoring applications.